Impact of collective excitations on direct pre-equilibrium emission: axially-symmetric-deformed nuclei

*M. Dupuis, S.Péru, E. Bauge and T. Kawano**
CEA, DAM, DIF

Abstract
A microscopic calculation of the first order of direct pre-equilibrium neutron emission for 10-20 MeV neutron scattering off ^{238}U is presented. Cross sections are obtained solving coupled channel equations. The JLM folding model is used to calculate the relevant coupling potentials. Spectroscopic information are calculated from the QRPA model with the Gogny D1S interaction. No arbitrary renormalization process enters our analyzes. Predictions are in good agreement with the data at high emission energy and illustrate the importance of the collective excitations in the modeling of the pre-equilibrium reaction mechanism for a deformed target.

1 Introduction

Pre-equilibrium models usually use adjustable parameters, so predictions cannot be easily extrapolated to domains where data are missing. Furthermore, some measurements have not yet been well explained: the high energy part of the neutron emission spectrum for neutron scattering on ^{238}U was only understood using a very empirical approach [1,2], that consists in adding fictitious collective levels in the low energy spectrum to describe the measured cross section. To improve the modeling of direct pre-equilibrium emission, we developed reaction models that only rely on a microscopic description of the target states, and that use realistic two-body interactions between the projectile and the target nucleons. In [3], a microscopic calculation of the direct pre-equilibrium neutron emission at first order was performed for neutron scattering off ^{90}Zr and ^{208}Pb. In this previous work, target excited states were described as one phonon excitations of the correlated Ground State (GS) predicted by the Random Phase Approximation (RPA) model. This approach, that describes on an equal footing direct inelastic scattering and direct pre-equilibrium emission (first step), provided an accurate description of the high energy neutron emission without any arbitrary normalization. It also demonstrated the importance of collective excitations for this reaction mechanism. In this work, we extend this approach to treat the case of axially deformed targets. Inelastic scattering cross sections are obtained solving coupled channel (CC) equations. The JLM convolution model [4] is used to calculate the diagonal potentials and the transition potentials corresponding to one phonon excitations. A Quasi-particle RPA (QRPA) calculation [5, 6] with the Gogny D1S interaction [7] has been performed to obtain the relevant spectroscopic information.

The theoretical description of direct pre-equilibrium emission is explained in Sec.2. In Sec. 3 we present the QRPA description of the target excitations. In Sec. 4, we explain the coupling scheme adopted in CC calculations and how coupling potentials are calculated, then we present and discuss the results obtained for ^{238}U. We give the conclusions and perspectives of this work in Sec.5.

2 Reaction theory

In the case of inelastic nucleon scattering, the double differential cross section for direct pre-equilibrium emission of a nucleon at the outgoing energy E_f in the range $[E_\mathrm{f}, E_\mathrm{f} + \Delta E]$ reads

$$\frac{d^2\sigma(\mathbf{k}_i, \mathbf{k}_f)}{d\Omega_\mathrm{f} dE_\mathrm{f}} = \frac{1}{\Delta E} \int_{E_f}^{E_\mathrm{f}+\Delta E} dE \sum_n f_n(E_\mathrm{i} - E - E_n) \frac{d\sigma_n(\mathbf{k}_i, \mathbf{k})}{d\Omega_\mathrm{f}} \,, \tag{1}$$

*Los Alamos National Laboratory

where $E_{\rm i} = \frac{k_i^2}{2\mu}$ is the nucleon incident energy, and $E = \frac{k^2}{2\mu}$. The differential cross section $\frac{d\sigma_n}{d\Omega}$ corresponds to the inelastic scattering to a discrete state of excitation energy E_n in the target nucleus. The distribution $f_n(E)$ accounts for the finite width (damping and escape) of this excitation. In [3], these individual cross sections were calculated within the DWBA approximation. For strongly deformed nuclei, it becomes necessary to use a coupled channel approach as very collective states lie at low energy.

To obtain the coupled channels equations for direct inelastic scattering to discrete states, one starts from the Schrödinger equation

$$(H-E)|\Psi\rangle = 0 \ , \ \ H = H_A + T + V \ , \tag{2}$$

where V is a two-body interaction acting between the projectile and the target nucleons, H_A the target Hamiltonian, and T the kinetic energy operator. We develop $|\Psi\rangle$ on the solutions $|n\rangle$ of H_A, namely $|\Psi\rangle = \sum_{n=0}^{\infty} u_n|n\rangle$, where u_n include the relative movement of the projectile and the target, and the spin+isospin wave functions of the projectile nucleon. We introduce the Feshbach projection operators

$$P = |0\rangle\langle 0| + \sum_{n=1}^{k} |n\rangle\langle n| \ , \ \ Q = \hat{1} - P = \sum_{m>k} |m\rangle\langle m| \ , \tag{3}$$

where the sum over n represents a finite set of target excited states, and $|0\rangle$ is the target GS. The definition of this set will be discussed later on. Applying these projection operators on (2), one gets the equation for $P|\Psi\rangle$:

$$(T + V_{\rm eff})\, P|\Psi\rangle = EP|\Psi\rangle \ , \ V_{\rm eff} = P\left(V + VQ\frac{1}{E - QHQ + i\eta}QV\right)P \ . \tag{4}$$

Projecting Eq.(4) on the GS $|0\rangle$ and the excited states $\{|n\rangle\}$ for $n \leq k$, one gets the set of coupled equations

$$(E_i - T_0 - U_{00})\,|u_0\rangle = \sum_{i=1}^{k} U_{0n}|u_n\rangle \ \text{ and } \ (E_f - T_0 - U_{nn})\,|u_n\rangle = \sum_{n'\neq n}^{k} U_{nn'}|u_{n'}\rangle \ \ \forall n \leq 4 \ , \tag{5}$$

where $E_{\rm f} = E_{\rm i} - E_n$. The coupling potentials $U_{nn'}$ are the matrix elements of the effective interaction between the target states, namely $U_{nn'} = (n|V_{\rm eff}|n')$. The parentheses mean integration over all the coordinates of the target nucleons. Individual cross sections for each inelastic channel are calculated from the solutions $|u_n\rangle$ of these equations.

3 QRPA description of the target excitations

A detailed presentation of the QRPA method and its implementation with the Gogny force is provided in [5]. We just remind here that axially-symmetric-deformed Hartree-Fock-Bogoliubov (HFB) calculations are performed imposing T, TP2, axial and left-right symmetry. Then the projection K of the angular momentum J on the symmetry axis and the parity π are good quantum numbers. In the QRPA formalism, the intrinsic excitations of the target are described as one phonon excitation of the correlated ground state $|0_I\rangle$, namely

$$|\alpha K^\pi\rangle = \Theta^+_{\alpha K^\pi}|0_I\rangle = \frac{1}{2}\sum_{ij\in(K^\pi)}\left(X_{ij}^{\alpha K^\pi}\eta^+_{ip_i\Omega_i}\eta^+_{jp_j\Omega_j} - (-)^K Y_{ij}^{\alpha K^\pi}\eta_{ip_i-\Omega_i}\eta_{jp_j-\Omega_j}\right)|0_I\rangle \ , \tag{6}$$

with $\Theta_{\alpha K^\pi}|0_I\rangle = 0$. For an even-even nucleus, the GS is such as $K^\pi = 0^+$. Two-quasiparticles (2-qp) unperturbed excitations of the uncorrelated HFB mean field $|HFB\rangle$ are defined as $|\beta K^\pi\rangle = \eta^+_{ip_i\Omega_i}\eta^+_{jp_h\Omega_j}|HFB\rangle$, where the projections Ω and the parities π of the quasi-particle creation operators

η^+ are such as $\Omega_i + \Omega_j = K$ and $p_i p_j = \pi$. Target states in the laboratory frame are obtained after projection over the total angular momentum

$$|\alpha JMK^\pi\rangle = \mathcal{N} \int d\Omega {\mathcal{D}^J_{MK}}^*(\Omega) R(\Omega) |\alpha K^\pi\rangle + (-)^{J+K} {\mathcal{D}^J_{M-K}}^*(\Omega) R(\Omega) |\alpha \bar{K}^\pi\rangle \ , \tag{7}$$

where $\mathcal{N}$ is a normalization factor, the $\mathcal{D}^J_{MK}$'s are rotation matrix elements, and $R(\Omega)$ is the rotation operator. For the GS and each excitation (6), we obtain a rotational band in the laboratory frame with total angular momenta and parities $J^\pi \geq K^\pi$ if $K > 0$, $J^\pi = 0^+,\ 2^+,\ 4^+$ ... if $K^\pi = 0^+$, and $J^\pi = 1^-,\ 3^-,\ 5^-$ ... if $K^\pi = 0^-$. Excitation energies of the states $|\alpha JMK^\pi\rangle$ are given by the approximation $E_{\alpha KJ\pi} = E_{\alpha K^\pi} + \frac{J(J+1)-K^2}{2\mathcal{I}}$, where the energies $E_{\alpha K^\pi}$ are the QRPA equations solutions, and $\mathcal{I}$ is the moment of inertia of the target in its GS.

We introduce the deformed radial GS density $\rho^{0_I,\alpha K^\pi}(\mathbf{r})$ and transition densities $\rho^{0_I,\alpha K^\pi}(\mathbf{r})$

$$\rho^{0_I}(\mathbf{r}) = \langle 0_I | \sum_{i=1}^{A} \delta(\mathbf{r} - \mathbf{r}_i) | 0_I \rangle \ \ , \ \ \rho^{0_I,\alpha K^\pi}(\mathbf{r}) = \langle \alpha K^\pi | \sum_{i=1}^{A} \delta(\mathbf{r} - \mathbf{r}_i) | 0_I \rangle \ . \tag{8}$$

where $\mathbf{r}_i$ is the coordinate of one of the target nucleons. The reduced transition probability of multipolarity $L \geq K$, associated to a transition between a state belonging to the GS band and a state belonging to a rotational band built on an intrinsic excitation of projection K and parity π, reads

$$B(E_L) \sim \int \rho^{0_I,\alpha K^\pi}_L(r) r^{L+2} dr \ \text{ for } \ L > 2 \ , \ \text{ with } \ \rho^{0_I,\alpha K^\pi}_L(r) = \int d\Omega \rho^{0_I,\alpha K^\pi}(\mathbf{r}) Y^L_K(\Omega) \ . \tag{9}$$

This relation holds in the case of a well deformed target for which the rotational approximation, defined as $\int d\Omega d\Omega' \equiv \int d\Omega \delta(\Omega - \Omega')$, applies.

QRPA calculations with the D1S interaction were performed for ^{238}U in a 13 harmonic oscillator major shells basis (see details in [6]). To characterize the collective content of the target spectrum predicted by the QRPA model, we compare the response functions (9) calculated with unperturbed 2-qp excitations, Fig. 1-(a), to those obtained with QRPA excitations, Fig. 1(b). The displayed $L = 3$ response functions correspond to all intrinsic excitations with total angular momentum projections $K \leq 3$. The QRPA response is considerably stronger than the unperturbed one for $E_n < 7$ MeV. It includes very collective transitions below 3 MeV, and two large peaks at 4.5 and 6.5 MeV that forms the Low Energy Octupole Resonance. Those differences between collective and unperturbed responses are also observed for the other angular momentum transfers up to L=8. As we will see, these collective excitations will strongly impact on the inelastic scattering predictions.

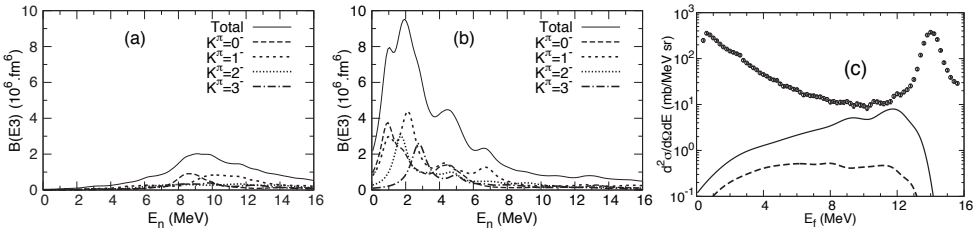

Fig. 1: (a) 2-qp and (b) QRPA $L = 3$ reduced transition probabilities in ^{238}U. Response functions have been folded with a 2 MeV-width Lorentz distribution. The different K components are labeled on the plots. Full black curves correspond to the sum over the K components. (c) Direct pre-equilibrium contribution to the (n,n') double differential cross-section at the outgoing angle $\theta_{c.m.} = 30°$, calculated with QRPA excitations (full curve) or 2-qp excitations (dashed curve), for 14.1 MeV neutron scattering on ^{238}U. The (n,*x*n) data are from [11].

4 Direct pre-equilibrium emission model for an axially-symmetric deformed target

4.1 Transition potentials and coupling scheme

In our approach, we represent the target spectrum with all the rotational bands built on each intrinsic excitation predicted by the QRPA model. All discrete inelastic scattering cross sections in (1) that correspond to the excitation of each of these states need to be calculated. Coupled channels calculations are performed coupling the rotational band built on the GS (GS band) to the rotational band built on a single intrinsic excitation (excited band). This calculation is repeated for each intrinsic excitation. The coupling potentials $U_{nn'}$ in Eq. (5) are calculated folding the QRPA radial densities (8) with a two-body effective interaction (4). In our applications, we use the folding method described in [4]. The JLM interaction as defined in [8] as been selected to represent the effective interaction. We precise that only direct potentials are used. As the JLM interaction was adjusted without considering knock-out exchange, its energy dependence is expected to approximately account for exchange effects.

The JLM interaction accounts for couplings to all non-elastic channels. Consequently, care should be taken when performing CC calculation. First, the imaginary part of the JLM interaction is reduced, as explained in [4], in order to compensate for the flux lost by the elastic channel when it is coupled to the inelastic channels of the GS band. Moreover, as this effective interaction is now adjusted to fit elastic and inelastic scattering to the GS band, it already includes, in principle, the couplings to all channels outside the GS band. Consequently, the couplings between excited bands are not included in our calculations. We remark that when we couple the GS band to one excited band, the effective interaction should also be renormalized to compensate for the additional absorption. However, as the flux in a single excited band remains small compared to the one in the GS band, we did not apply any additional renormalization.

The approximation of the present model, that limits the coupling to a single excited band, may be discussed as opening the couplings to more excitations may perturb the angular distributions calculated for the different inelastic channels. Note that if such a calculation was performed, the effective interaction should be renormalized each time the coupling scheme is extended. However, as we are interested in the direct pre-equilibrium emission cross-section that corresponds to a sum of many contributions, results should not be too sensitive to the details of individual inelastic channels.

4.2 Results for ^{238}U

We present the direct pre-equilibrium cross-sections (1) calculated with the model described in the previous section. All the intrinsic excitations with $K^{\pm} = 0^{\pm}$ to $8^{\pm}$ predicted by the QRPA model are included in the calculations. The coupled equations (5) are solved with the the code ECIS [9]. Rotational band states (7) are considered up to a total angular momentum $J = 8$, and the coupling potentials in Eq. (5) up to an orbital angular momentum transfer $L = 8$. These truncations ensure a good convergence of the calculations. The spreading functions $f_n(E)$ in Eq. (1) are obtained with the method used in Ref. [3].

Figure 1(c) displays the neutron spectrum for 14.1 MeV neutron scattering off ^{238}U at the emission angle $\theta_{c.m.} = 30°$. On this plot, the direct pre-equilibrium (n,n') cross-sections calculated with QRPA excitations and 2-qp excitations are compared. The cross-section obtained with QRPA excitations is considerably larger, following the behavior of response functions discussed in Sec.3. This illustrates the impact of collective transitions that are not described with 2-qp excitations.

We display on Fig. 2 the QRPA pre-equilibrium emission along with contributions to the (n,xn) cross sections arising from other reaction mechanisms, namely elastic scattering and inelastic scattering to the GS band states, evaporation from the Compound Nucleus (CN) and from the fission fragments. These other contributions are calculated following the method described in [10]. Predictions are compared to (n,xn) experimental data for the three incident energies 11.8 MeV, 14.1 MeV and 18 MeV, and the three outgoing angles $\theta_{c.m.} = 30°$, $90°$ and $120°$. We discuss the displayed spectra in term of excitation energies, namely $E^* = E_{\rm i} - E_{\rm f}$. We first focus on the high energy part of the spectra that corresponds to $E^* < 4$ MeV. At the three displayed incident energies, the predicted cross sections are

almost always in good agreement with the data. In previous analyzes [1, 2], the high energy emission was always underestimated by the pre-equilibrium calculations, and empirical collective states were introduced to obtain a good fit of the experimental cross sections. The present result proves what was postulated in these empirical analyzes: collective transitions, which are now predicted from a well established nuclear structure model, have to be included to describe correctly the direct neutron emission. Exceptions to this good agreement are observed at $E_{\rm i} = 11.8$ and 14.1 MeV for $\theta_{c.m.} = 30^{\circ}$. In the first case, data are largely underestimated only for $E^* = 1 - 2$ MeV. The shape of the experimental elastic peak suggests that a distribution broader than the Gaussian shape assumed in the present calculation should be used. This may improve agreement with the data at high emission energy. In the second case, predictions lie 20% below the data for $E^* = 1 - 4$ MeV This discrepancy is hard to interpret. Studies with other targets at the same incident energy should be perform to test if the same discrepancy remains. At energies E^* =4-9 MeV for $E_{\rm i} = 14.1$, and E^* =4-12 MeV for $E_{\rm i} = 18$ MeV, our predictions clearly underestimate the data. This is discussed in the next section.

4.3 Discussion

In neutron induced reactions, the high energy neutron emission is known to come from a direct inelastic scattering process that excites discrete states in the target. Moreover, the most part of this contribution comes from vibrational collective states which are well described with one phonon excitations predicted by the (Q)RPA model. The good agreement with the data at high emission energy confirms that the excitation of one phonon states, limited to natural parity transitions, is correctly described in the present approach. Thus, as our model does not involve any arbitrary renormalization process, we can state that the discrepancy between our calculations and the data observed a lower emission energy comes from other important reaction mechanisms that are either missing in the present analysis or not well described. First, non-natural parity excitations, that produce up to 20% of the direct pre-equilibrium cross-section for neutron scattering on ^{208}Pb (see [3]), are not yet included. The excitation of two-phonons states via a one or a two-steps process could also provide a non negligible contribution. A good treatment of these two mechanisms could reduced the discrepancy with the data. As seen on Fig.2, evaporation from fission fragments provides non-negligible neutron emission cross sections in the same energy range than the direct pre-equilibrium emission. As this contribution is calculated from a phenomenological model, different parameters set and/or approximations could eventually improve the agreement with the data. In our analysis, we have neglected the Multi-Step Compound (MSC) pre-equilibrium emission mechanism. However, the magnitude of the calculated cross-section varies greatly between different MSC model implementations. A careful study of this process, based on microscopic ingredients, should be performed to measure its actual contribution to the neutron emission.

5 Conclusions

We have presented a microscopic calculation of direct pre-equilibrium emission for 10-20 MeV neutron scattering off the axially deformed nucleus ^{238}U. Our model is based on a microscopic description of the target states, limited to one phonon excitations, provided by the QRPA model implemented with the Gogny D1S interaction. We demonstrate that the large collective content of the target spectrum predicted by the QRPA model allows us to explain the direct neutron emission observed a high energy. Our model does not include any arbitrary renormalization process. However, discrepancies between the predicted cross sections and data appear at lower emission energy and need to be understood. First, the present study is being extended to other targets to provide a better overview of the present model qualities. Non-natural-parity transitions will soon be included in the calculation and effect of two-phonons transitions on the direct pre-equilibrium cross section will also be studied. The description of other reaction mechanisms, such as MSC and evaporation from fission fragments, should also be improved.

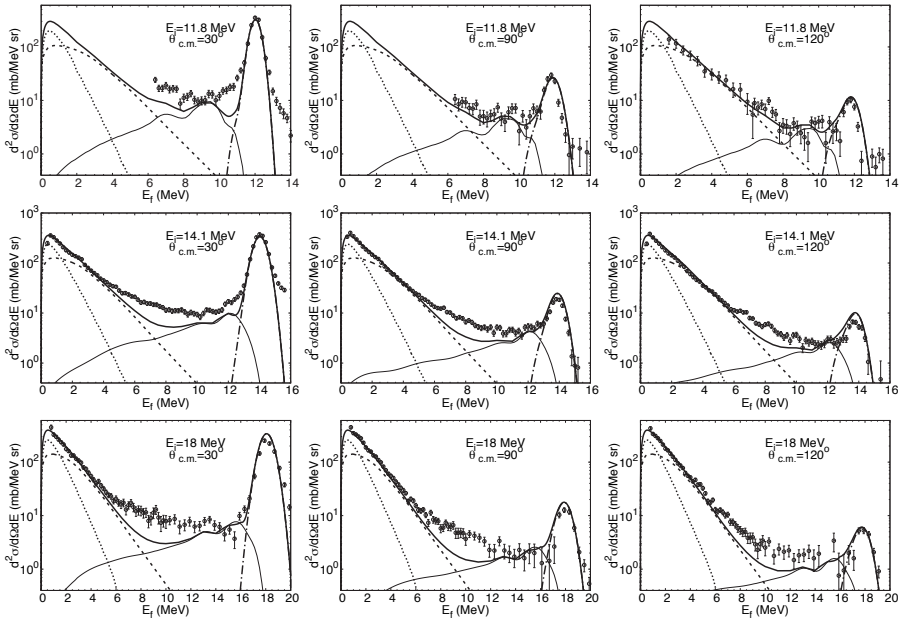

Fig. 2: Double differential (n,xn) cross sections for a ^{238}U target. Incident energies $E_{\rm i}$ and outgoing angles $\theta_{c.m.}$ are given on each plot. Thin full curves correspond to the direct pre-equilibrium emission calculated with QRPA excitations, dashed curves to the evaporation from fission fragments, dotted curves to the evaporation from the CN, dashed-dotted curves to the elastic scattering and inelastic scattering to the GS band states, and thick full curves to the sum of these contributions. Open circles represent data from [11–13].

Acknowledgments

We wish to thank J.-P. Delaroche for enlightening discussions and J. Raynal for his constant support with the code ECIS.

References

[1] T. Miura, M. Baba M. Ibaraki et al, Annals of Nuclear Energy **28**, 937 (2000).

[2] M. Chadwick et al, Nuclear Data Sheets **107**, 2931 (2006).

[3] M. Dupuis, T. Kawano, J.-P. Delaroche and E. Bauge, Phys.Rev.C **83**, 014602 (2011).

[4] E. Bauge et al., Phys.Rev.C **61**, 034306 (2000).

[5] S. Péru and H. Goutte, Phys. Rev. C **78**, 024305 (2008).

[6] S. Peru et al., Phys.Rev.C **83**, 014314 (2011).

[7] J.F. Berger, M. Girod and D. Gogny Comp.Phys.Comm. **63**, 365 (1991).

[8] E. Bauge, J.-P. Delarcoche and M. Giraud, Phys.Rev.C **63**, 024607 (2001).

[9] J.Raynal, CEA report No.CEA-N-2772, 1994.

[10] T. Kawano, T. Ohsawa, M. Baba and T. Nakagawa, Phys. Rev. C, **63**, 034601 (2001)

[11] M. Baba, H. Wakabayashi, N. Ito, K. Maeda and N. Irakawa, J. Nucl. Sci. Technol. **27**, 601 (1990).

[12] M. Baba et al., in *proc. of Int. Conf. on Nuclear Data for Science and Technology*, Jülich, Germany, 1991, edited by S. M. Qaim (Springer-Verlag, Berlin/Heidelberg, 1992), p.349.

[13] Shen Guanren et al,Chinese Physics **8**, 1000 (1988).